Published in final edited form as:
Nature. 2011 June 2; 474(7349): 54–60. doi:10.1038/nature10139.

Principles of activation and permeation in an anion-selective Cys-loop receptor

Ryan E. Hibbs[1] and **Eric Gouaux**[1,2]

[1]Vollum Institute, Oregon Health and Science University, 3181 SW Sam Jackson Park Road, Portland OR 97239 USA

[2]Howard Hughes Medical Institute, Oregon Health and Science University, 3181 SW Sam Jackson Park Road, Portland OR 97239 USA

Summary

Fast inhibitory neurotransmission is essential for nervous system function and is mediated by binding of inhibitory neurotransmitters to receptors of the Cys-loop family embedded in the membranes of neurons. Neurotransmitter binding triggers a conformational change in the receptor, opening an intrinsic chloride channel, thereby dampening neuronal excitability. We present the first 3D structure of an inhibitory anion-selective Cys-loop receptor, the homopentameric *Caenorhabditis elegans* glutamate-gated chloride channel α (GluCl), at 3.3 Å. The X-ray structure of the GluCl-Fab complex was determined with the allosteric agonist ivermectin and in additional structures with the endogenous neurotransmitter L-glutamate and the open-channel blocker picrotoxin. Ivermectin, used to treat river blindness, binds in the transmembrane domain of the receptor and stabilizes an open pore conformation. Glutamate binds in the classical agonist site at subunit interfaces, and picrotoxin directly occludes the pore near its cytosolic base. GluCl provides a framework for understanding mechanisms of fast inhibitory neurotransmission and allosteric modulation of Cys-loop receptors.

Introduction

Fast inhibitory neurotransmission modulates both the magnitude and duration of neuronal activity, occurs on a timescale of milliseconds, and involves the release of inhibitory neurotransmitters into the synapse and activation of the cognate ligand-gated ion channels. As demonstrated nearly 60 years ago[1], fast inhibitory neurotransmission leads to an increase in the permeability of the cell membrane to chloride, the most abundant biological anion. Because the membrane potential at which chloride is at equilibrium is near the neuronal resting potential, neurotransmitter-gated, chloride-selective ion channels generally oppose normal excitability and repolarize the cell[2].

The neurotransmitter receptors that directly mediate chloride permeability constitute one half of the Cys-loop receptor family[3]. Receptors in this family are composed of five either identical or homologous subunits, which generate diversity in functional profiles and pharmacological preferences. Cys-loop receptors fall into two broad categories. The cation-

Correspondence and requests for materials should be addressed to E.G. (gouauxe@ohsu.edu).

Supplementary Information is linked to the online version of the paper at www.nature.com/nature.

Author Contributions R.E.H. and E.G. contributed to all aspects of the project.

Author Information Atomic coordinates and structure factors have been deposited with the Protein Data Bank under codes 3RHW, 3RIF, 3RI5 and 3RIA for the GluCl-Fab-ivermectin, +glutamate, +picrotoxin and +iodide structures, respectively.

selective members are the nicotinic acetylcholine (nAChR) and serotonin 5-HT_3 receptors. Those selective for anions include the γ-amino butyric acid ($GABA_{A/C}$), glycine receptors and invertebrate glutamate-gated chloride channels (GluCl)[3–6]. There is to date no structural information for an anion-selective Cys-loop receptor, and the mechanism by which chloride is selected remains unclear.

Ligand-gated chloride channels are critical not only for maintaining appropriate neuronal activity, but have long been important therapeutic targets: benzodiazepines, barbiturates, some intravenous and volatile anesthetics, alcohol, strychnine, picrotoxin and ivermectin all derive their biological activity from acting on the inhibitory half of the Cys-loop receptor family[3,7]. Of note is that many of the therapeutically useful compounds acting at Cys-loop receptors target an allosteric site. The sites in Cys-loop receptors at which these allosteric ligands bind and their structure-based mechanisms of action are largely unresolved.

Crystallization of GluCl-Fab complex

We identified the *Caenorhabditis elegans* GluClα glutamate-gated chloride channel[8] as a promising candidate using fluorescence-detection size-exclusion chromatography (FSEC)[9]. In comparison to human Cys-loop receptors, GluClα is most similar to the α1 glycine receptor, with which it shares 34% amino acid sequence identity (see alignment in Supplementary Figure 1). Optimization of the receptor construct for crystallization ($GluCl_{cryst}$) was guided by FSEC analysis and required deletion of 41 residues from the amino terminus, 6 residues from the carboxy terminus and replacement of the M3/M4 loop (Lys345-Lys402) with an Ala-Gly-Thr tripeptide. Well ordered crystals diffracting to ~3.3 Å resolution required co-crystallization of $GluCl_{cryst}$ as a complex with a Fab, ivermectin and lipids (Supplementary Figure 2). Structures with agonist or channel blocker at 3.3 and 3.4 Å were obtained by soaking $GluCl_{cryst}$-Fab-ivermectin crystals with glutamate or picrotoxin, respectively. The electron density maps are of high quality, thus enabling the positioning of almost all receptor residues and refinement to satisfactory crystallographic residuals and stereochemistry (Supplementary Table 1 and Supplementary Figure 3).

Architecture

The $GluCl_{cryst}$-Fab complex forms a pinwheel shape comprising a cylindrical homopentamer of $GluCl_{cryst}$ subunits with Fab molecules bound at each subunit interface (Figure 1a-b). Each $GluCl_{cryst}$ subunit consists of a large amino-terminal extracellular domain (ECD) of mostly β structure, followed by four α-helical TM spans (M1-M4, Figure 1c). The overall architecture of the ECD is similar to that found in the bacterial receptor orthologs from *Gleobacter violaceus* (GLIC)[10,11] and *Erwinia chrysanthemi* (ELIC)[12]. There is an additional helix at the amino terminus reminiscent of the acetylcholine binding protein[13–15] (AChBP) and *Torpedo marmorata* nAChR[16] structures. Significantly, GluCl contains the Cys-loop disulfide strictly conserved in eukaryotes as well as a disulfide bond in loop C present in glycine receptors (Figure 1c). The TM helices adopt a fold like the bacterial receptors and nAChR, with the five M2 segments lining the pore and adopting an open channel conformation, akin to the conformation visualized in the GLIC structures.

To understand the molecular principles of ion channel activation, agonist binding and ion channel permeation and block, we determined separate crystal structures with the allosteric agonist ivermectin, and with ivermectin and glutamate, picrotoxin or iodide. Ivermectin is bound at each of the $GluCl_{cryst}$ subunit interfaces in the TM domain whereas glutamate electron density is present in all five of the classical neurotransmitter binding sites in the ECD. Anomalous difference density for iodide is present in sites at the base of the TM pore in a region important for ion selectivity, and a chloride ion was fit into non-protein electron density in the ion channel pore adjacent to the binding site for picrotoxin.

Allosteric activation and modulation

Ivermectin is a semi-synthetic macrocyclic lactone and broad spectrum antiparasitic agent, widely used to treat river blindness in humans and parasitic infections in animals[17,18]. It achieves its margin of therapeutic efficacy by activating invertebrate glutamate-gated chloride channels at nanomolar concentrations[8,19], yet it also manifests activating and potentiating activities on vertebrate Cys-loop receptors[20–22] and on P2X ATP-gated ion channels[23] at higher concentrations. Ivermectin potently activates GluClα (Supplementary Figure 4) while simultaneously rendering the receptor susceptible to further activation by glutamate[24]. Hence, at GluClα, we deem ivermectin a partial allosteric agonist.

Ivermectin binds at subunit interfaces on the periphery of the TM domains, proximal to the extracellular side of the membrane bilayer (Figure 2a-b and Supplementary Figures 5-7). Wedged between the M3 α-helix on the principal or (+) subunit and the M1 α-helix on the complementary or (-) subunit, ivermectin inserts deeply into the subunit interface and makes important contacts with the M2 (+) pore-lining α-helix and the M2/M3 loop. Its site occupies ~2 turns of helix on the M1 and M3 helices and centers on a single turn of π-helix between residues Leu217 and Ile222 on M1, as illustrated by a hydrogen bond between the main chain carbonyl oxygen of Leu218 and a tertiary hydroxyl on ivermectin. Through extensive hydrophobic interactions and one hydrogen bond with each of the M1, M2 and M3 α-helices, ivermectin buries 278 and 254 $Å^2$ of surface area on the (+) and (-) subunits in the interface, respectively.

Ser260 forms a hydrogen bond with the secondary hydroxyl group on the deeply buried cyclohexene ring of ivermectin (Figure 2a-c, Supplementary Figure 8). A serine residue in this position is correlated with direct activation by ivermectin in other Cys-loop receptors. Glycine and $GABA_A$ receptors have a serine in the equivalent position and are directly activated by ivermectin[20,21], yet there is no similar serine in α7 nAChRs, where ivermectin is a positive allosteric modulator but does not directly activate[22], nor in GluClβ receptors, where ivermectin has no activity[8]. The equivalent position is critical for $GABA_A$ receptor modulation by alcohol[25], anticonvulsants, anesthetics and diuretics; glycine and $5\text{-}HT_3$ receptor modulation by anesthetics[6]; and α7 nAChR modulation by additional compounds[26]. Hence, the ivermectin binding site in $GluCl_{cryst}$ is shared, at least in part, by many important modulators of Cys-loop receptors. In GluCl we suspect that the interaction of ivermectin with the pore-lining M2 helix increases both its affinity for the receptor and its ability to stabilize the open state.

Ivermectin binding to GluCl likely results in two types of conformational changes: first, a local distortion of the receptor in the vicinity of the binding site, and second, a global conformational change of the receptor that corresponds to a transition from a closed, resting state to an open, activated state. Because we lack a structure of $GluCl_{cryst}$ in the absence of ivermectin, GLIC provides a reference for gauging the local structural consequences of ivermectin binding to the transmembrane domain of the receptor. In comparing these two structures we find that the binding of ivermectin increases the separation between M1 and M3 of adjacent subunits, as defined by a 9.4 Å spacing between $GluCl_{cryst}$ Leu218 and Gly281 Cα atoms compared to 6.4 Å spacing for the corresponding atoms in GLIC. This splaying apart of the TM helices in $GluCl_{cryst}$ occurs at the level of a strictly conserved proline residue in M1 that forms the carboxy terminal end of the short π-helix (Supplementary Figure 9).

We hypothesize that the global conformational change induced by ivermectin binding is rooted in the splaying apart of the M1 and M3 helices and the movement of the apical portion of M2 away from the pore axis, toward the periphery of the receptor, opening an ion

conductive pathway. This open-pore conformation of M2 is then stabilized through interactions between ivermectin and the apical end of M2. In addition, ivermectin may stabilize the open state of the ion channel through contacts between the disaccharide moiety and Ile273 in the M2/M3 loop (Supplementary Figure 10).

Neurotransmitter binding site

The ion channel of $GluCl_{cryst}$ is activated by glutamate only following activation by ivermectin (Supplementary Figure 11), in a manner similar to full length GluClα[24]. The homomeric GluClβ and heteromeric GluClαβ receptors, by contrast, are directly activated by glutamate[8]. In the context of $GluCl_{cryst}$, micromolar concentrations of glutamate augment ivermectin-induced currents by 30-70%, similar to that of full length receptor. [^{3}H]-L-glutamate binds directly to the $GluCl_{cryst}$ receptor with a K_D of 680 nM (Supplementary Figures 11-13). In agreement with the electrophysiology experiments, [^{3}H]-L-glutamate binding requires ivermectin. To understand the molecular basis of glutamate binding we determined the structure of $GluCl_{cryst}$ in the presence of ivermectin and glutamate. Sausage-shaped electron density assigned to glutamate was ~8σ in F_{obs}-F_{calc} omit maps in all five of the classical agonist binding sites. Omit electron density maps subjected to real space, 5-fold averaging displayed a protrusion in the electron density 'sausage' that we attributed to the α-amino group of glutamate (Supplementary Figure 14).

Glutamate binds in the classical neurotransmitter site in the ECD[3,27], lodged between subunits and nearly inaccessible to solvent (Figure 3a-b). The architecture of the site is box-like, with loops from the (+) subunit forming 'sides' of the binding site and the β-strands on the (-) subunit defining the 'base.' Loop C, postulated to play a critical role in allosteric activation[15,28–30], adopts a closed conformation consistent with AChBP structures bound by agonists. Functional groups on glutamate bridge the (+) and (-) subunits with the α-substituents snugly sandwiched between Tyr151 and Tyr200 on the (+) subunit, and positively charged residues, including Arg37 from a region important for conotoxin-nAChR interaction[31], and Arg56 on the (-) subunit, making contacts with the α- and γ-carboxylate groups. These arginine residues, in combination with neighboring cationic amino acids, provide the binding pocket with a strongly positive electrostatic potential (Supplementary Figure 15). The α-amino nitrogen of glutamate is stabilized through a 3.8 Å cation-π interaction with Tyr200 on loop C, a hydrogen bond with the backbone carbonyl oxygen of Ser150 and a close interaction with the backbone carbonyl oxygen of Tyr151. A comparison of the determinants of glutamate binding with the corresponding residues in the AChBPs and other receptors is made in Supplementary Figure 16.

To test the sensitivity of the glutamate binding site to perturbations in ligand structure, we screened glutamate analogs for competition with [^{3}H]-L-glutamate bound to the ivermectin-complexed receptor (Figure 3c, Supplementary Figure 17). L-glutamate bound much tighter than L-homocysteine sulfinic acid, which differs only in replacement of Cδ with sulfur. Extending the side chain length with an extra carbon (L-amino adipic acid) or shortening it (L-aspartate) resulted in a further drop in affinity, and changing the stereochemistry (D-glutamate) or removing the side chain negative charge but not its ability to hydrogen bond (L-glutamine) decreased binding further. Thus, the GluCl neurotransmitter binding pocket is selective for small dicarboxylate L-amino acids, consistent with the constellation of atomic interactions between agonist and receptor (Figure 3a-b).

Upon the binding of glutamate the side chain of Arg56 in loop D (β2) shifts by ~0.5 Å to accommodate the agonist and Tyr200 in loop C repositions by ~0.5 Å closer to the ligand, small yet significant conformational changes consistent with movements of loops C and D in the agonist-induced activation of the receptor. These residues, together with Arg37 (β1), are

located on elements of protein structure directly connected to the ion channel pore. We suggest that ivermectin, a partial allosteric agonist, stabilizes an 'activated' conformation of the agonist site and that binding of glutamate to this 'activated' site further stabilizes the open state of the receptor, increasing chloride conductance. How does ivermectin transduce a conformational change to the neurotransmitter site? Perhaps through the interactions of ivermectin with the M2/M3 loop, located at the structural nexus of three ECD loops central to allosteric communication between the neurotransmitter site in the ECD and the TM pore: the Cys-, β1/β2 and β8/β9 loops[6] (Figure 2a, Supplementary Figure 10). Hydrophobic residues in the M2/M3 loop mediating these interactions are well conserved in most Cys-loop receptors, consistent with the M2/M3 loop playing a central role in the activation mechanism of receptors throughout the family[32–36].

Pore conformation

To test the hypothesis that the $GluCl_{cryst}$-ivermectin structure represents an open, conducting conformation (Figure 4), we carried out functional and structural studies using picrotoxin, an open channel blocker[37,38] (Figure 5, Supplementary Figure 18). Electron density in picrotoxin-soaked crystals was apparent at a position near the cytosolic side of the transmembrane pore, on the 5-fold axis of molecular symmetry (4.3 σ, Supplementary Figure 19). Thus, the observed electron density is an average of five orientations. Nevertheless, the egg-shaped picrotoxin-associated electron density suggests that the basket-like, fused tricyclic rings are directed extracellularly and near 2′Thr, while the isoprenyl tail points toward the cytoplasm and is proximal to -2′Pro residues. In this position, the majority of the oxygen atoms of picrotoxin are cradled by the polar belt of 2′Thr hydroxyls while the hydrophobic isoprenyl moiety is surrounded by the methylene groups of the non-polar -2′Pro side chains. Most importantly, the binding of picrotoxin to the pore of $GluCl_{cryst}$-ivermectin complex reinforces our hypothesis that the pore is an open conformation.

The smallest diameter of the $GluCl_{cryst}$ ion channel pore is ~4.6 Å, defined by a hydrophobic 'girdle' of -2′Pro side chains proximal to the cytoplasmic side of the membrane. Because chloride has a Pauling radius of 1.8 $Å^2$, passage of chloride, iodide (Pauling radius of 2.2 $Å^2$) and other permeant ions through the -2′Pro constriction must involve substantial dehydration, in agreement with previous studies demonstrating a correlation between energies of hydration and relative permeabilities (higher for iodide than chloride, Supplementary Figure 20)[39]. The pore constriction in $GluCl_{cryst}$ is somewhat smaller than that estimated for $GABA_A$, glycine and GluClβ receptors (5.2-6.2 Å)[3,40], based on low but measureable relative permeability to ions like acetate, gluconate and phosphate. This difference may be due to the alanine residues at the -2′ position in the β subunits of all three of those receptors.

GluCl is related to the *Torpedo* nAChR (PDB: 2BG9)[16] in amino acid sequence and three dimensional structure and thus we compared the structures and the aligned sequences. In so doing, we found inconsistencies between amino acid sequence-based alignments and three-dimensional structure-based alignments of the M2 and M3 α-helices. A similar finding was described in comparisons of GLIC to the nAChR[4]. Our analysis indicates that in the α-subunit M2 pore-lining helix and the M3 α-helix, the nAChR amino acid assignment is off in register by 4 residues or ~1 turn of an α-helix beginning with the M1/M2 loop (Supplementary Figure 21).

Ion selectivity

Analysis of $GluCl_{cryst}$ surface electrostatics reveals an electropositive vestibule, a slightly electronegative extracellular half of the TM pore, and an electropositive intracellular half (Figure 6a). None of the pore-lining residues in $GluCl_{cryst}$ bear a formal charge and thus the

positive electrostatic potential at the base of the pore arises from the oriented peptide dipoles in the M2 α-helices[41], reminiscent of the role that helical dipoles play in ClC chloride channels[42]. Cation channels reverse the selectivity imposed by orientation of the M2 dipoles through placing a negatively charged side chain near the pore constriction point[43]. While other regions contribute to the modulation of conductance and selectivity in some Cys-loop receptors, the minimal determinants of selectivity are the -1′Ala and -2′Pro positions for anions and the -1′Glu for cations[3,44], with no requirement for positively charged amino acids in the pore of anion-selective channels[40] (Supplementary Figure 22).

To identify sites important in chloride binding and selectivity, we soaked crystals of $GluCl_{cryst}$ in iodide, a heavy atom analog of chloride, and observed four anomalous difference peaks that we ascribe to iodide, located at the cytosolic base of the TM pore and centered around the 5-fold symmetry axis (Figure 6b-d). The weak density at the fifth site is simply the consequence of an interfering lattice contact with an adjacent Fab. Each iodide sits in a concave pocket of positive electrostatic potential formed by -2′Pro residues from the M2 helices of adjacent subunits, main chain backbone atoms of -1′Ala and -3′Ile and the methyl group of -1′Ala. All three of these residues are important in selectivity for some receptors, with the -1′ position being an essential component of selectivity across the family[3]. Previous studies suggest that the main chain amide nitrogen at the -3′ position is important in GluClβ receptors for anion dehydration[40]. In $GluCl_{cryst}$ this atom is ~5 Å from the center of the iodide anomalous density and could form water-mediated hydrogen bonds to anions at the mouth of the ion channel pore.

Electron density maps derived from all $GluCl_{cryst}$ X-ray diffraction data sets exhibit a spherical peak in the pore between the 2′Thr and 6′Thr residues (6.8 σ in F_{obs}-F_{calc} omit maps) with no other peaks in the pore above 2.5 σ. Anomalous difference electron density maps were inconclusive in identification of this peak. Therefore, we placed several different ions or molecules in the difference density and determined, through crystallographic refinement and inspection of difference electron density maps, that a single chloride anion best accounted for this electron density feature (Supplementary Table 1). Distances between the modeled chloride and 6′Thr side chain hydroxyl oxygen atoms are consistent with water mediated hydrogen bonding of chloride in the pore[45], indicating this location could be a transiently occupied ion binding site flanking the constriction point. Further experimentation is required to validate the chemical identity of the bound species.

The iodide binding sites nestled in electropositive pockets at the base of the pore suggest general principles of ion selectivity in Cys-loop receptors. In GluCl and other chloride-selective receptors there is either an alanine or glycine residue at the -1′ position of the M2 helix, thus preserving the concave pocket. By contrast, in eukaryotic cation selective channels, the -1′ residue is a conserved glutamate. We suggest that the carboxylate side chain of glutamate not only fills the ‘anion pocket’ but that it also imposes a local negative electrostatic potential important for cation selectivity (Supplementary Figure 22). Previous cysteine accessibility studies in cation selective channels have suggested that the -1′Glu position lines the TM pore[46]. However, on the basis of the $GluCl_{cryst}$ structure and amino acid sequence alignments, we propose that the preceding residue, a conserved glycine (-2′ residue), lines the pore of cation channels, consistent with the significantly larger pore diameter of cation channels (7.4-8.4 Å). In support of the -2′ residue defining the pore constriction, deletion of the -2′Pro in glycine receptors, which would shift the following glycine residue into the -2′ position, increases pore diameter to 6.9 Å[47]. Furthermore, the -2′Gly position in cation-selective 5-HT_{3A} receptors is accessible to modification when the pore is open[48]. We propose that the -2′ position lines the pore in both anion and cation channels and that the ‘anion pockets’ in $GluCl_{cryst}$ are important determinants of ion selectivity, increasing the local concentration of anions at the cytoplasmic mouth of the pore.

Conclusion

Here we present the first X-ray structure of a eukaryotic Cys-loop receptor, a glutamate-gated chloride channel from *C. elegans*. $GluCl_{cryst}$ was co-crystallized with ivermectin, a partial allosteric agonist that sequesters within the membrane bilayer and binds to exposed sites on the transmembrane domains of the receptor. Lipophilic modulators of other Cys-loop receptors may exploit a similar mechanism of interaction, including the neurosteroids at the $GABA_A$ receptor[6] and cholesterol at the muscle nAChR[49]. The $GluCl_{cryst}$-ivermectin structure maps a previously uncharacterized binding site at a protein-lipid interface and defines a protein/chemical scaffold for design of receptors and ligands with new pharmacological properties and receptor specificities. Binding of ivermectin induces local changes in the membrane domain and global conformational changes in the entire receptor, pre-organizing the agonist binding site ~30 Å away and opening the ion channel pore. Analysis of amino acids lining and proximal to the pore suggest that anion selectivity is accomplished largely through a pore constriction imposed by proline residues and a positive electrostatic potential, conferred by the amino terminal end of the M2 helix dipoles. These new findings advance our understanding of the molecular mechanism of fast neuronal inhibition, the importance of which was first appreciated more than one hundred years ago[50].

Methods summary

$GluCl_{cryst}$ was expressed from baculovirus-infected Sf9 cells and purified by metal ion affinity chromatography. The Fab complex was isolated by size-exclusion chromatography. The $GluCl_{cryst}$-Fab complex was concentrated to 1-2 mg/mL and supplemented with synthetic lipids and ivermectin. Crystallization was performed by hanging drop vapor diffusion at 4°C with a precipitating solution containing 21-23% PEG 400, 50 mM sodium citrate pH 4.5 and 70 mM sodium chloride. Cryoprotection was achieved by soaking crystals in precipitant solution supplemented with 30% PEG 400. Additional complexes were obtained by soaking crystals in cryoprotectant containing L-glutamate, picrotoxin or sodium iodide. Diffraction data were indexed, integrated and scaled and the structure solved by molecular replacement using a GLIC-derived homology model of $GluCl_{cryst}$ and a Fab homology model as search probes. The molecular replacement phases were used to initiate autobuilding and the resulting model was iteratively improved by cycles of manual adjustment and crystallographic refinement. Function of GluCl was examined by two-electrode voltage clamp experiments and by [^{3}H]-L-glutamate saturation and competition binding assays.

Full Methods

Construct design

The gene encoding the full-length *C. elegans* GluClα protein (GI:1091780)[8], including the native signal peptide and a C-terminal 8×-histidine tag, was codon optimized and subcloned into the pFastBac1 vector for baculovirus-driven expression in Sf9 insect cells. A construct for FSEC[9]-based small-scale screening of detergent stability, mutagenesis, and purification additionally contained the EGFP-coding sequence inserted into the M3/M4 loop region as previously described[51-53]. To improve crystallization behavior, 41 amino acid residues from the N-terminus and 6 from the C-terminus were removed, and residues K345-K402 (in the mature, full-length sequence), corresponding to the M3/M4 loop, were substituted with the residues AGT.

GluCl expression and purification

Bacmid and baculovirus were generated from pFastBac1 constructs and Sf9 cells were infected at 27°C using standard methods. After 18 h of infection, cells were maintained shaking at 20°C, and then harvested for purification after 72-96 h. Cells were collected by centrifugation at 6,200 × g and disrupted using an EmulsiFlex-C5 (Avestin) in buffer containing 20 mM Tris pH 7.4, 150 mM NaCl (TBS buffer), and 1 mM PMSF. The homogenate was clarified by centrifugation at 9,700 × g, and crude membranes were collected from the light membrane fraction by centrifugation at 125,000 × g (at r_{avg}). The membranes were mechanically homogenized and solubilized in 0.25 g $C_{12}M$ (*n*-dodecyl-β-D-maltopyranoside, Anatrace) per g of membranes in TBS. Solubilized membranes were centrifuged at 125,000 × g. Supernatant containing $GluCl_{cryst}$ was bound to TALON Co^{2+}-affinity resin (Clontech), washed with TBS solution containing 1 mM $C_{12}M$ and 25 mM imidazole, and eluted with 250 mM imidazole. All purification steps were performed at 4°C.

Monoclonal antibody generation and Fab purification

The mouse monoclonal antibody against GluCl (IgG1, λ) was obtained using standard methods[54]. Specificity of the antibody for properly-folded pentameric $GluCl_{cryst}$ was assayed by FSEC and Western blot. Cloning and sequencing of Fab antibody regions were performed from mouse hybridoma cells. Antibody was purified from hybridoma supernatants by cation exchange and protein A affinity chromatography. Fab fragments were generated by papain digest of whole antibody, and purified by protein A chromatography to remove Fc molecules and undigested material, followed by anion exchange.

Purification of $GluCl_{cryst}$-Fab complex

Eluent from Co^{2+}-affinity purification and Fab from ion exchange were mixed to an excess of Fab to $GluCl_{cryst}$ subunits, concentrated, and applied to a gel filtration column (Superose 6 10/300 GL, GE Healthcare Life Sciences) equilibrated in TBS + 1 mM $C_{12}M$. $GluCl_{cryst}$ - Fab complex was concentrated to 1-2 mg/mL. For samples used in crystallization, 1-palmitoyl-2-oleoyl-*sn*-glycero-3-phosphocoline (POPC) or 1,2-dipalmitoyl-*sn*-glycero-3-phosphocoline (DPPC) lipids (Avanti Polar Lipids) were added to 0.02% from a 2% stock suspension in 20% DMSO, 80% gel filtration buffer, and ivermectin (Sigma) was added to 0.1 mM from a 10 mM stock in DMSO.

Crystallization and cryoprotection

Initial crystallization attempts of GluCl constructs in the absence of Fab resulted in poorly diffracting (8 Å) crystals that grew in a very limited range of crystallization conditions. Crystallization of the Fab complex occurred in diverse conditions; best diffracting crystals were obtained in hanging-drop format and diffracted to 4-5 Å. Crystals diffracting beyond 4 Å were obtained only in the presence of Fab, either POPC or DPPC, and ivermectin. These tetragonal crystals grew by vapor diffusion at 4°C in 21-23% PEG 400, 50 mM sodium citrate pH 4.5, and 70 mM sodium chloride, and diffracted maximally to Bragg spacings of 3.26 Å (Supplementary Table 1). Crystals were protected before flash freezing in liquid nitrogen by 1-2 min soaks in crystallization solution supplemented to contain 30% PEG 400. To obtain structures of $GluCl_{cryst}$ in complex with additional ligands, crystals of the same form were soaked briefly in cryoprotectant containing either 5 mM picrotoxin (picrotoxinin, the more active component of picrotoxin, was used, obtained from Sigma), 50 mM L-glutamate or 300 mM sodium iodide. In an effort to minimize occupancy of chloride in the iodide-soaked crystals, crystals were transferred serially into three replicate cryoprotectant solutions lacking chloride before flash freezing. Nonetheless, because the iodide soaks were only 1-2 minutes, some chloride may have been carried over from crystallization. Electron density maps derived from these crystals showed no significant change in the strength of the

electron density feature in the pore where we have modeled a chloride ion. We also soaked crystals in an analogous manner in bromide-containing cryo-solutions but were not able to observe significant peaks in the resultant anomalous difference electron density maps.

Data collection

Diffraction data were collected using synchrotron radiation at the Advanced Photon Source (Argonne National Laboratory, beamline 24-ID-C) with a mini-Kappa goniometer and in-house crystal alignment strategy software. The best-ordered crystals have a diffraction limit of 3.26 Å, a mosaic spread of 0.2-0.5°, and they are of the space group $P4_32_12$ with one $GluCl_{cryst}$ -Fab complex per asymmetric unit. The unit cell dimensions are $a = b = 155$ Å, $c = 575$ Å, $\alpha = \beta = \gamma = 90°$, resulting in a Matthews' coefficient (V_M) of 4.0 $Å^3/Da$[55]. Diffraction data were indexed, integrated and scaled using HKL2000[56] or Xia2[57-62] software.

Structure determination

The structure was solved by molecular replacement using Phaser[63]; the search probe was a pentameric homology model of $GluCl_{cryst}$ made from GLIC (PDB: 3EHZ)[10], using Swiss-Model[64]. After an initial solution was found, phases were improved by solvent flattening[65] and electron density for Fab molecules bound at each of the five subunit interfaces of $GluCl_{cryst}$ became plainly visible. A Fab homology model was made, using PDB 1NGQ for the light chain and 1F3D for the heavy chain, and Coot[66] to overlay the two modeled chains to make a single Fab molecule. Fab CDR loops were truncated and the model was used for molecular replacement using the $GluCl_{cryst}$ solution as a starting point. In this manner, a single Fab was placed, and by copying the remaining Fab molecules around the 5-fold non-crystallographic symmetry (NCS) axis, approximate positioning of all Fab molecules was accomplished. Electron density for Fab constant domain regions was poor after NCS averaging, and from non-averaged maps it was clear that the Fab constant domains did not obey 5-fold symmetry. A starting model that included $GluCl_{cryst}$ and five Fab variable domains was used for automated building with Buccaneer[67]. Electron density maps were then good enough to position ivermectin molecules in the transmembrane domain loci, and to begin manual building of the Fab constant domains. Ivermectin stereochemistry, determined previously, is modeled as such[68]. Numbering of ivermectin atoms in the figures is as defined in the PDB files; Supplementary Table 2 relates this numbering to that from the small molecule structure.

Iterative refinement of the model against the X-ray data using Phenix[69], manual adjustment in Coot into simulated annealing composite omit electron density maps[69] or real-space averaged maps[70], and structure quality analysis using Molprobity[71] were carried out until satisfactory model statistics were obtained. Three groups of five-fold NCS restraints were present during refinement: five subunits of $GluCl_{cryst}$, five heavy chain Fab variable domains (residues 1-120), and the five light chain Fab variable domains (residues 1-108); the r.m.s. deviations between the chains within each of these three groups were 0.017, 0.014, and 0.015 Å, respectively. Isotropic B factors and TLS parameters were also refined; the 15 TLS groups comprised five $GluCl_{cryst}$ subunits, five Fab variable domains, and five Fab constant domains. The final models contain the $GluCl_{cryst}$ pentamer from residues 1-339 or 340, five ivermectin molecules, a single N-linked carbohydrate at N185 in three of the five subunits, five Fab molecules (1-221 for heavy chains, 1-210 for light chains), and several lipid and detergent molecules. Some portions of the Fab constant domains lacked electron density in composite omit maps and hence were omitted from the final model. The iodide-bound structure is of very low resolution and not completely refined: several anomalous difference electron density peaks in the ECD were not modeled with iodide atoms.

Sequence alignments were made using PROMALS3D[72] and ClustalW[73]. Isoelectric surface calculations were made using the APBS[74] add-on in PyMOL[75]. Pore dimensions were analyzed using HOLE software[76].

Electrophysiology

RNAs encoding GluCl proteins were transcribed from pGEM-HE[77] plasmids using the mMessage mMachine T7 Ultra kit (Ambion). Defolliculated stage V-VI *Xenopus* oocytes were generously provided by David C. Dawson and Chris Alexander, prepared as previously described[78]. Oocytes were injected with 25 ng of GluCl RNAs, and current recordings were made 3-5 days following. Frog saline (FS) recording solution contained (mM) 96 NaCl, 2 KCl, 1 $MgCl_2$, 1.8 $CaCl_2$, 5 Hepes pH 7.5. Recording solution for iodide permeability experiments was FS but with NaI in place of NaCl. All ligands were made up in FS from stock solutions in water, except: picrotoxin, 1 M stock in DMSO; ivermectin, 5 mM stock in DMSO. Recording electrode pipettes (0.7-2 MΩ) were cushioned with 0.8% LMP agarose in 3 M KCl and backfilled with 3 M KCl. Oocytes were voltage-clamped at -80 mV except in experiments to determine the reversal potential which employed 40 ms voltage steps. Analog data were filtered at 50 Hz and digitized at ≥1 kHz. The Axoclamp 2B amplifier (Axon Instruments) and pClamp 10 software (Molecular Devices) were used for data acquisition. In uninjected oocytes, no significant responses to test solutions were observed (Supplementary Figure 13).

Radioligand binding experiments

Experiments to test binding of [^{3}H]-L-glutamate to $GluCl_{cryst}$ and competition of the radioligand with other compounds were done using purified Nano15-tagged[79] $GluCl_{cryst}$ (N-terminal tag) and streptavidin-Ysi scintillation proximity assay beads (SPA; GE Healthcare Life Sciences). The concentration of binding sites was fixed at 100 nM after a preliminary experiment to determine optimal $GluCl_{cryst}$ concentration (Supplementary Figure 12). Other binding assay components were: 50 mM Tris pH 7.4, 150 mM NaCl, 1 mM $C_{12}M$, 1 mg/mL SPA beads, and 1 μM ivermectin. Saturation binding of [^{3}H]-L-glutamate in the presence and absence of Fab was performed with a 1:30 dilution of specific activity of the radiolabel with [^{1}H]-L-glutamate, and a slight molar excess of Fab to $GluCl_{cryst}$ binding sites as verified by FSEC experiments. Measurement of background signal in saturation binding experiments was complicated by, we believe, significant binding of [^{3}H]-L-glutamate directly to SPA beads and lack of a chemically-distinct competitor for the neurotransmitter binding site. Neither high concentrations of [^{1}H]-L-glutamate or absence of protein were able to fully account for this apparently non-specific signal. To address the background component that was not accurately measured experimentally, we combined subtraction of a background signal measured in the absence of $GluCl_{cryst}$ with a linear component still present in the binding data (calculated using the total binding function in the fitting software). In saturation binding experiments in the presence of Fab (Supplementary Figure 12), data were better fit after removing background signal measured in the presence of 10 mM [^{1}H]-L-glutamate combined with the calculated linear component. In competition binding experiments to determine IC_{50} values, [^{3}H]-L-glutamate was 1 μM using a 1:10 dilution of specific activity of the radiolabel with cold glutamate. In all [^{3}H]-L-glutamate and electrophysiological dose-response experiments, data were fit with GraphPad Prism software.

Supplementary Material

Refer to Web version on PubMed Central for supplementary material.

Acknowledgments

We are grateful to Henry Lester for providing the initial GluCl construct, to Dan Cawley for monoclonal antibody production, to Jennifer Michel for Fab fragment cloning and sequencing, to Chris Alexander and David C. Dawson for generously providing *Xenopus* oocytes, to Mark Mayer for advice and equipment related to oocyte experiments, and to Lori Vaskalis for help with illustrations. We thank the staff at the Advanced Photon Source beamline 24-ID-C for assistance with X-ray data collection. We are particularly appreciative of helpful discussion with Gouaux lab members and Ed McCleskey. This work was supported by an individual NIH National Research Service Award (F32NS061404) to R.E.H. E.G. is an investigator with the Howard Hughes Medical Institute.

References

1. Coombs JS, Eccles JC, Fatt P. The specific ionic conductances and the ionic movements across the motoneuronal membrane that produce the inhibitory post-synaptic potential. J Physiol. 1955; 130:326–374. [PubMed: 13278905]
2. Hille, B. Ion Channels of Excitable Membranes. Sinauer Associates, Inc.; Sunderland, MA: 2001.
3. Thompson AJ, Lester HA, Lummis SC. The structural basis of function in Cys-loop receptors. Q Rev Biophys. 2010; 43:449–499. [PubMed: 20849671]
4. Corringer PJ, et al. Atomic structure and dynamics of pentameric ligand-gated ion channels: new insight from bacterial homologues. J Physiol. 2010; 588:565–572. [PubMed: 19995852]
5. Hilf RJ, Dutzler R. A prokaryotic perspective on pentameric ligand-gated ion channel structure. Curr Opin Struct Biol. 2009; 19:418–424. [PubMed: 19646860]
6. Miller PS, Smart TG. Binding, activation and modulation of Cys-loop receptors. Trends Pharmacol Sci. 2010; 31:161–174. [PubMed: 20096941]
7. Garcia PS, Kolesky SE, Jenkins A. General Anesthetic Actions on GABA(A) Receptors. Curr Neuropharmacol. 2010; 8:2–9. [PubMed: 20808541]
8. Cully DF, et al. Cloning of an avermectin-sensitive glutamate-gated chloride channel from *Caenorhabditis elegans*. Nature. 1994; 371:707–711. [PubMed: 7935817]
9. Kawate T, Gouaux E. Fluorescence-detection size-exclusion chromatography for precrystallization screening of integral membrane proteins. Structure. 2006; 14:673–681. [PubMed: 16615909]
10. Hilf RJ, Dutzler R. Structure of a potentially open state of a proton-activated pentameric ligand-gated ion channel. Nature. 2009; 457:115–118. [PubMed: 18987630]
11. Bocquet N, et al. X-ray structure of a pentameric ligand-gated ion channel in an apparently open conformation. Nature. 2009; 457:111–114. [PubMed: 18987633]
12. Hilf RJ, Dutzler R. X-ray structure of a prokaryotic pentameric ligand-gated ion channel. Nature. 2008; 452:375–379. [PubMed: 18322461]
13. Brejc K, et al. Crystal structure of an ACh-binding protein reveals the ligand-binding domain of nicotinic receptors. Nature. 2001; 411:269–276. [PubMed: 11357122]
14. Celie PH, et al. Crystal structure of acetylcholine-binding protein from *Bulinus truncatus* reveals the conserved structural scaffold and sites of variation in nicotinic acetylcholine receptors. J Biol Chem. 2005; 280:26457–26466. [PubMed: 15899893]
15. Hansen SB, et al. Structures of *Aplysia* AChBP complexes with nicotinic agonists and antagonists reveal distinctive binding interfaces and conformations. Embo J. 2005; 24:3635–3646. [PubMed: 16193063]
16. Unwin N. Refined structure of the nicotinic acetylcholine receptor at 4Å resolution. J Mol Biol. 2005; 346:967–989. [PubMed: 15701510]
17. Campbell WC, Fisher MH, Stapley EO, Albers-Schonberg G, Jacob TA. Ivermectin: a potent new antiparasitic agent. Science. 1983; 221:823–828. [PubMed: 6308762]
18. Aziz MA, Diallo S, Diop IM, Lariviere M, Porta M. Efficacy and tolerance of ivermectin in human onchocerciasis. Lancet. 1982; 2:171–173. [PubMed: 6123884]
19. Arena JP, Liu KK, Paress PS, Cully DF. Avermectin-sensitive chloride currents induced by *Caenorhabditis elegans* RNA in *Xenopus* oocytes. Mol Pharmacol. 1991; 40:368–374. [PubMed: 1716730]

20. Adelsberger H, Lepier A, Dudel J. Activation of rat recombinant alpha(1)beta(2)gamma(2S) GABA(A) receptor by the insecticide ivermectin. Eur J Pharmacol. 2000; 394:163–170. [PubMed: 10771281]
21. Shan Q, Haddrill JL, Lynch JW. Ivermectin, an unconventional agonist of the glycine receptor chloride channel. J Biol Chem. 2001; 276:12556–12564. [PubMed: 11278873]
22. Krause RM, et al. Ivermectin: a positive allosteric effector of the alpha7 neuronal nicotinic acetylcholine receptor. Mol Pharmacol. 1998; 53:283–294. [PubMed: 9463487]
23. Silberberg SD, Li M, Swartz KJ. Ivermectin Interaction with transmembrane helices reveals widespread rearrangements during opening of P2X receptor channels. Neuron. 2007; 54:263–274. [PubMed: 17442247]
24. Etter A, Cully DF, Schaeffer JM, Liu KK, Arena JP. An amino acid substitution in the pore region of a glutamate-gated chloride channel enables the coupling of ligand binding to channel gating. J Biol Chem. 1996; 271:16035–16039. [PubMed: 8663156]
25. Ueno S, Wick MJ, Ye Q, Harrison NL, Harris RA. Subunit mutations affect ethanol actions on GABA(A) receptors expressed in *Xenopus* oocytes. Br J Pharmacol. 1999; 127:377–382. [PubMed: 10385236]
26. Young GT, Zwart R, Walker AS, Sher E, Millar NS. Potentiation of alpha7 nicotinic acetylcholine receptors via an allosteric transmembrane site. Proc Natl Acad Sci U S A. 2008; 105:14686–14691. [PubMed: 18791069]
27. Kao PN, et al. Identification of the alpha subunit half-cystine specifically labeled by an affinity reagent for the acetylcholine receptor binding site. J Biol Chem. 1984; 259:11662–11665. [PubMed: 6480577]
28. Damle VN, Karlin A. Effects of agonists and antagonists on the reactivity of the binding site disulfide in acetylcholine receptor from *Torpedo californica*. Biochemistry. 1980; 19:3924–3932. [PubMed: 7407078]
29. Celie PH, et al. Nicotine and carbamylcholine binding to nicotinic acetylcholine receptors as studied in AChBP crystal structures. Neuron. 2004; 41:907–914. [PubMed: 15046723]
30. Mukhtasimova N, Free C, Sine SM. Initial coupling of binding to gating mediated by conserved residues in the muscle nicotinic receptor. J Gen Physiol. 2005; 126:23–39. [PubMed: 15955875]
31. Quiram PA, McIntosh JM, Sine SM. Pairwise interactions between neuronal alpha(7) acetylcholine receptors and alpha-conotoxin PnIB. J Biol Chem. 2000; 275:4889–4896. [PubMed: 10671525]
32. Lee WY, Sine SM. Principal pathway coupling agonist binding to channel gating in nicotinic receptors. Nature. 2005; 438:243–247. [PubMed: 16281039]
33. Campos-Caro A, et al. A single residue in the M2-M3 loop is a major determinant of coupling between binding and gating in neuronal nicotinic receptors. Proc Natl Acad Sci U S A. 1996; 93:6118–6123. [PubMed: 8650229]
34. Kusama T, Wang JB, Spivak CE, Uhl GR. Mutagenesis of the GABA rho 1 receptor alters agonist affinity and channel gating. Neuroreport. 1994; 5:1209–1212. [PubMed: 7919166]
35. Lynch JW, Rajendra S, Barry PH, Schofield PR. Mutations affecting the glycine receptor agonist transduction mechanism convert the competitive antagonist, picrotoxin, into an allosteric potentiator. J Biol Chem. 1995; 270:13799–13806. [PubMed: 7775436]
36. Rajendra S, et al. Mutation of an arginine residue in the human glycine receptor transforms beta-alanine and taurine from agonists into competitive antagonists. Neuron. 1995; 14:169–175. [PubMed: 7826634]
37. Takeuchi A, Takeuchi N. A study of the action of picrotoxin on the inhibitory neuromuscular junction of the crayfish. J Physiol. 1969; 205:377–391. [PubMed: 5357245]
38. Etter A, et al. Picrotoxin blockade of invertebrate glutamate-gated chloride channels: subunit dependence and evidence for binding within the pore. J Neurochem. 1999; 72:318–326. [PubMed: 9886084]
39. Fatima-Shad K, Barry PH. Anion permeation in GABA- and glycine-gated channels of mammalian cultured hippocampal neurons. Proc Biol Sci. 1993; 253:69–75. [PubMed: 7690484]
40. Sunesen M, et al. Mechanism of Cl- selection by a glutamate-gated chloride (GluCl) receptor revealed through mutations in the selectivity filter. J Biol Chem. 2006; 281:14875–14881. [PubMed: 16527818]

41. Wada A. The alpha-helix as an electric macro-dipole. Adv Biophys. 1976:1–63. [PubMed: 797240]
42. Dutzler R, Campbell EB, Cadene M, Chait BT, MacKinnon R. X-ray structure of a ClC chloride channel at 3.0 A reveals the molecular basis of anion selectivity. Nature. 2002; 415:287–294. [PubMed: 11796999]
43. Wilson GG, Pascual JM, Brooijmans N, Murray D, Karlin A. The intrinsic electrostatic potential and the intermediate ring of charge in the acetylcholine receptor channel. J Gen Physiol. 2000; 115:93–106. [PubMed: 10653890]
44. Keramidas A, Moorhouse AJ, Schofield PR, Barry PH. Ligand-gated ion channels: mechanisms underlying ion selectivity. Prog Biophys Mol Biol. 2004; 86:161–204. [PubMed: 15288758]
45. Mancinelli R, Botti A, Bruni F, Ricci MA, Soper AK. Hydration of sodium, potassium, and chloride ions in solution and the concept of structure maker/breaker. J Phys Chem B. 2007; 111:13570–13577. [PubMed: 17988114]
46. Akabas MH, Kaufmann C, Archdeacon P, Karlin A. Identification of acetylcholine receptor channel-lining residues in the entire M2 segment of the alpha subunit. Neuron. 1994; 13:919–927. [PubMed: 7524560]
47. Lee DJ, Keramidas A, Moorhouse AJ, Schofield PR, Barry PH. The contribution of proline 250 (P-2′) to pore diameter and ion selectivity in the human glycine receptor channel. Neurosci Lett. 2003; 351:196–200. [PubMed: 14623139]
48. Reeves DC, Goren EN, Akabas MH, Lummis SC. Structural and electrostatic properties of the 5-HT3 receptor pore revealed by substituted cysteine accessibility mutagenesis. J Biol Chem. 2001; 276:42035–42042. [PubMed: 11557761]
49. Barrantes FJ. Structural basis for lipid modulation of nicotinic acetylcholine receptor function. Brain Res Brain Res Rev. 2004; 47:71–95. [PubMed: 15572164]
50. Sherrington, CS. Integrative Action of the Nervous System. Yale University Press; New Haven: 1906.
51. Gensler S, et al. Assembly and clustering of acetylcholine receptors containing GFP-tagged epsilon or gamma subunits: selective targeting to the neuromuscular junction in vivo. Eur J Biochem. 2001; 268:2209–2217. [PubMed: 11298737]
52. Li P, Slimko EM, Lester HA. Selective elimination of glutamate activation and introduction of fluorescent proteins into a *Caenorhabditis elegans* chloride channel. FEBS Lett. 2002; 528:77–82. [PubMed: 12297283]
53. Slimko EM, Lester HA. Codon optimization of *Caenorhabditis elegans* GluCl ion channel genes for mammalian cells dramatically improves expression levels. J Neurosci Methods. 2003; 124:75–81. [PubMed: 12648766]
54. Harlow, E.; Lane, D. Antibodies: A Laboratory Manual. Cold Spring Harbor Laboratory Press; Cold Spring Harbor: 1988.
55. Matthews BW. Solvent content of protein crystals. J Mol Biol. 1968; 33:491–497. [PubMed: 5700707]
56. Otwinowski Z, Minor W. Processing of X-ray diffraction data collected in oscillation mode. Macromolecular Crystallography Pt A. 1997:307–326.
57. The CCP4 suite: programs for protein crystallography. Acta Crystallogr D Biol Crystallogr. 1994; 50:760–763. [PubMed: 15299374]
58. Evans P. Scaling and assessment of data quality. Acta Crystallogr D Biol Crystallogr. 2006; 62:72–82. [PubMed: 16369096]
59. Leslie AGW. Joint CCP4 and ESF-EAMCB Newsletter on Protein Crystallography 26. 1992
60. Leslie AG. The integration of macromolecular diffraction data. Acta Crystallogr D Biol Crystallogr. 2006; 62:48–57. [PubMed: 16369093]
61. Sauter NK, Grosse-Kunstleve RW, Adams PD. Robust indexing for automatic data collection. J Appl Crystallogr. 2004; 37:399–409. [PubMed: 20090869]
62. Zhang CY, Sauter NK, van den Bedem H, Snell G, Deacon AM. Automated diffraction image analysis and spot searching for high-throughput crystal screening. J Appl Cryst. 2006; 39:112–119.

63. McCoy AJ, et al. Phaser crystallographic software. J Appl Crystallogr. 2007; 40:658–674. [PubMed: 19461840]
64. Arnold K, Bordoli L, Kopp J, Schwede T. The SWISS-MODEL workspace: a web-based environment for protein structure homology modelling. Bioinformatics. 2006; 22:195–201. [PubMed: 16301204]
65. Cowtan K. Joint CCP4 and ESF-EACBM Newsletter on Protein Crystallography. 1994; 31:34–38.
66. Emsley P, Cowtan P. Coot: Model-Building Tools for Molecular Graphics. Acta Crystallogr. 2004; (Section D):2126–2132.
67. Cowtan K. The Buccaneer software for automated model building. 1. Tracing protein chains. Acta Crystallogr D Biol Crystallogr. 2006; 62:1002–1011. [PubMed: 16929101]
68. Springer JP, Arison BH, Hirshfield JM, Hoogsteen K. The Absolute Stereochemistry and Conformation of Avermectin B2a Aglycon and Avermectin B1a. J Am Chem Soc. 1981; 103:4221–4221.
69. Adams PD, et al. PHENIX: a comprehensive Python-based system for macromolecular structure solution. Acta Crystallogr D Biol Crystallogr. 2010; 66:213–221. [PubMed: 20124702]
70. The CCP4 Suite: Programs for Protein Crystallography. Acta Crystallogr. 1994:760–776.
71. Chen VB, et al. MolProbity: all-atom structure validation for macromolecular crystallography. Acta Crystallogr D Biol Crystallogr. 2009; 66:12–21. [PubMed: 20057044]
72. Pei J, Kim BH, Grishin NV. PROMALS3D: a tool for multiple protein sequence and structure alignments. Nucleic Acids Res. 2008; 36:2295–2300. [PubMed: 18287115]
73. Thompson JD, Higgins DG, Gibson TJ. CLUSTAL W: improving the sensitivity of progressive multiple sequence alignment through sequence weighting, position-specific gap penalties and weight matrix choice. Nucleic Acids Res. 1994; 22:4673–4680. [PubMed: 7984417]
74. Baker NA, Sept D, Joseph S, Holst MJ, McCammon JA. Electrostatics of nanosystems: application to microtubules and the ribosome. Proc Natl Acad Sci U S A. 2001; 98:10037–10041. [PubMed: 11517324]
75. DeLano, W. L. (DeLano Scientific, San Carlos, CA, USA, 2002).
76. Smart OS, Goodfellow JM, Wallace BA. The pore dimensions of gramicidin A. Biophys J. 1993; 65:2455–2460. [PubMed: 7508762]
77. Liman ER, Tytgat J, Hess P. Subunit stoichiometry of a mammalian K+ channel determined by construction of multimeric cDNAs. Neuron. 1992; 9:861–871. [PubMed: 1419000]
78. Alexander C, et al. Cystic fibrosis transmembrane conductance regulator: using differential reactivity toward channel-permeant and channel-impermeant thiol-reactive probes to test a molecular model for the pore. Biochemistry. 2009; 48:10078–10088. [PubMed: 19754156]
79. Lamla T, Erdmann VA. The Nano-tag, a streptavidin-binding peptide for the purification and detection of recombinant proteins. Protein Expr Purif. 2004; 33:39–47. [PubMed: 14680960]

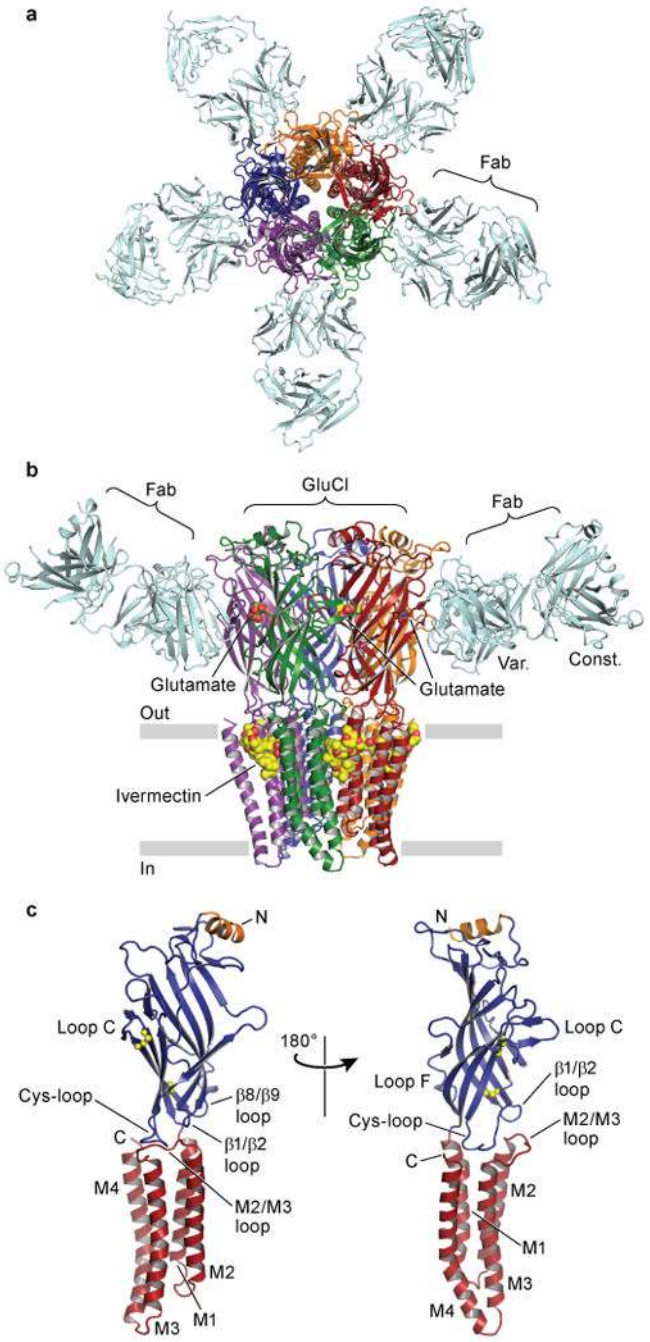

Figure 1. Architecture of $GluCl_{cryst}$-Fab complex

In **a**, view of the $GluCl_{cryst}$-Fab complex looking down pore axis toward cytosol. Fab molecules (cyan) are bound at each $GluCl_{cryst}$ subunit interface. In **b**, view parallel to lipid membrane; only two Fab molecules are shown for clarity. The ligands ivermectin and glutamate are represented as spheres with carbon atoms in yellow, oxygen in red and nitrogen in blue. In **c**, a single $GluCl_{cryst}$ subunit from two angles, approximate orientation as in panel **b**. The Cys-loop and loop C disulfide bonds are shown as spheres, N- and C-termini and TM spans are indicated. Loops of particular relevance to agonist binding and allosteric gating linkage are also indicated.

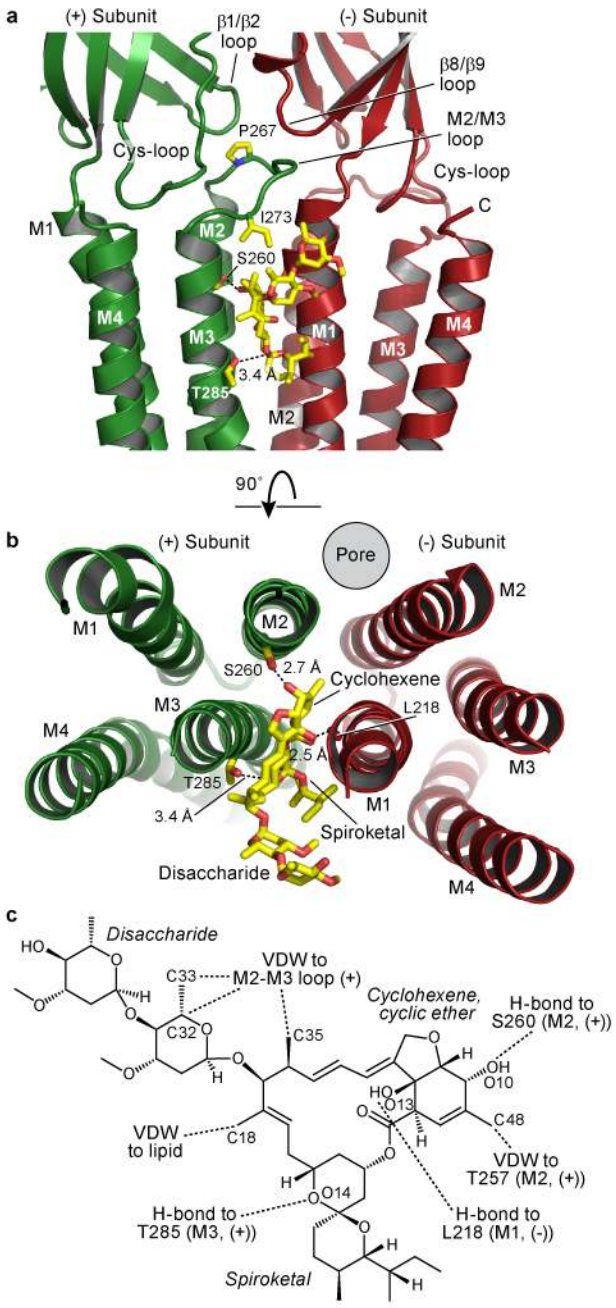

Figure 2. Ivermectin binding site and atomic interactions

In **a** and **b**, two orientations of a GluCl subunit interface focusing on ivermectin binding site. Dashed lines indicate hydrogen bonds. In **a**, view is from receptor periphery looking parallel to the membrane, and in **b** looking down pore from extracellular side with ECD removed for clarity. In **c**, chemical structure of ivermectin with interactions indicated; VDW: van der Waals. Atomic numbering is from PDB file.

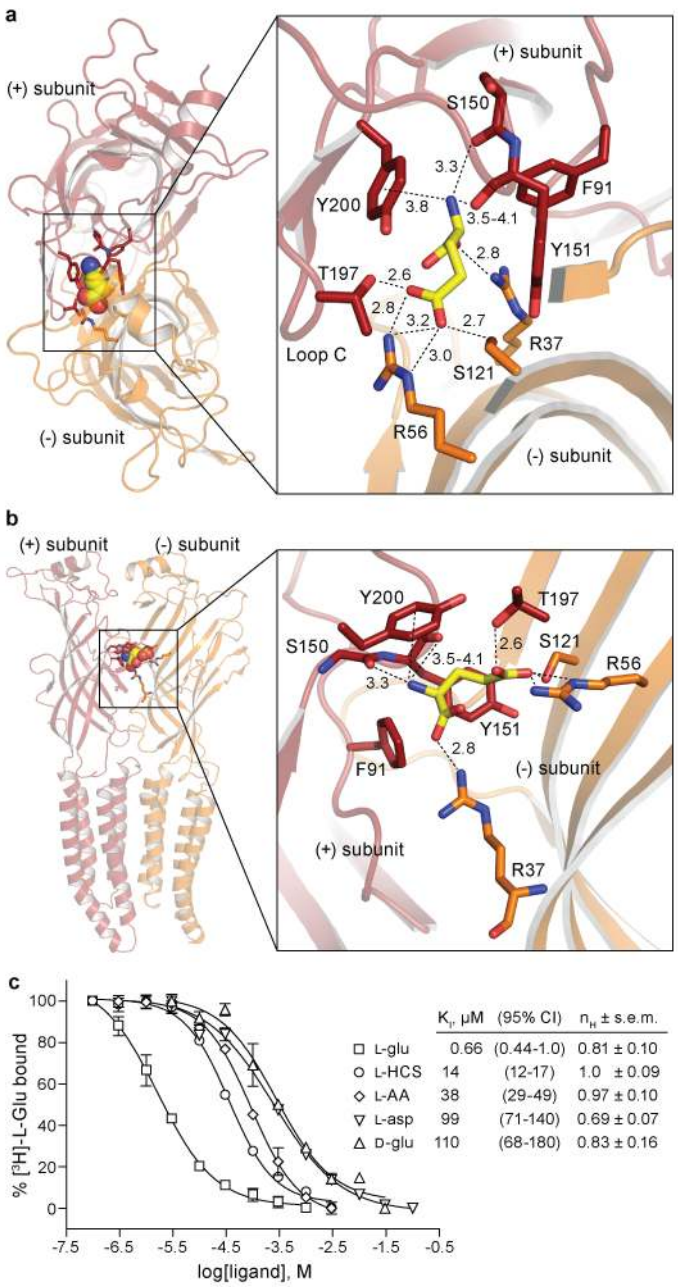

Figure 3. Glutamate binding site and specificity

In **a**, view from extracellular side toward membrane at glutamate in binding site in subunit interface. In **b**, view of binding site looking parallel to membrane with loop C removed for clarity. Dashed lines with distances in Å indicate hydrogen bonding and, in the case of Tyr200, cation-π interactions. Unless a range is given, distances are an average from the five binding sites. In **c**, radioligand competition experiments with L-glutamate and congeners against 1 mM [^{3}H]-L-glutamate. Calculated K_I values assume a K_D for [^{3}H]-L-glutamate of 680 nM and are shown in inset table; $n = 2$ and CI, confidence interval. L-HCS and L-AA are L-homocysteine sulfinic acid and L-amino adipic acid, respectively.

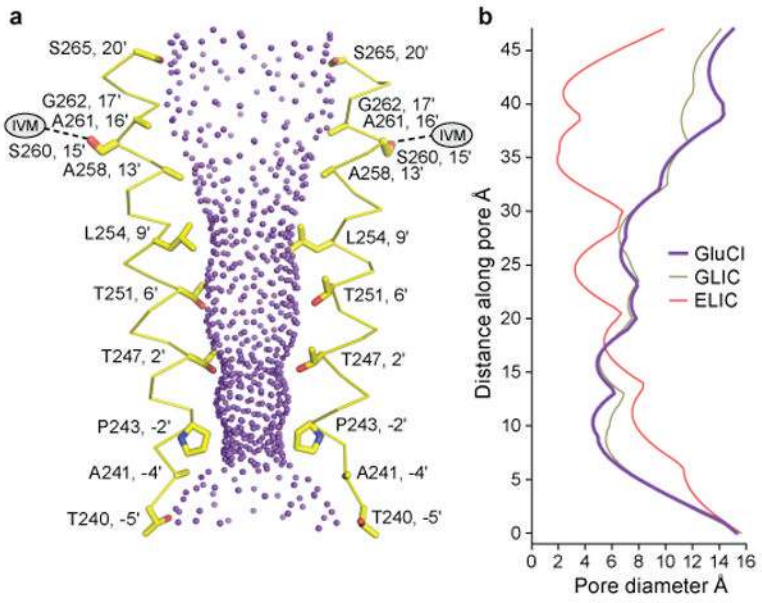

Figure 4. Ion channel

In **a**, purple spheres represent internal surface of transmembrane ion channel, with side chains shown for pore-lining residues from two of the five M2 α-helices that line the pore; Ser260 does not line the pore but hydrogen bonds with ivermectin. In **b**, pore diameter is plotted as a function of longitudinal distance along the pore for $GluCl_{cryst}$, open (GLIC, PDB: 3EAM) and closed (ELIC: 2VL0) bacterial receptors.

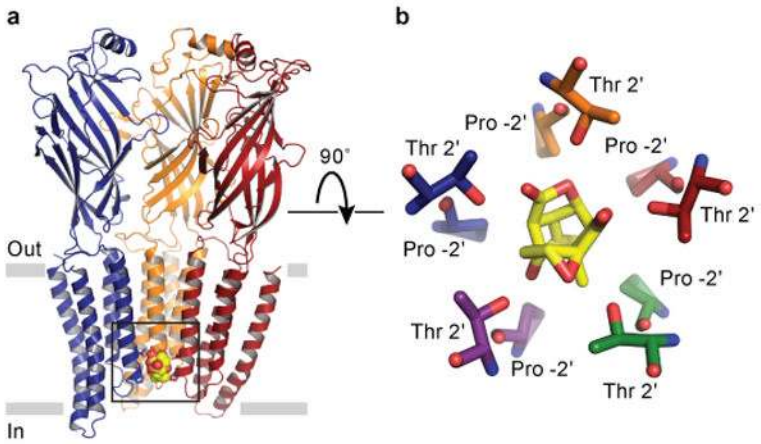

Figure 5. Picrotoxin binding site

In **a**, front two subunits removed to show picrotoxin location (boxed) at cytosolic base of pore. Residues involved in picrotoxin binding are shown as sticks and van der Waals surfaces are shown for picrotoxin. In **b**, looking into pore from ECD at picrotoxin position relative to 2′Thr and -2′Pro side chains.

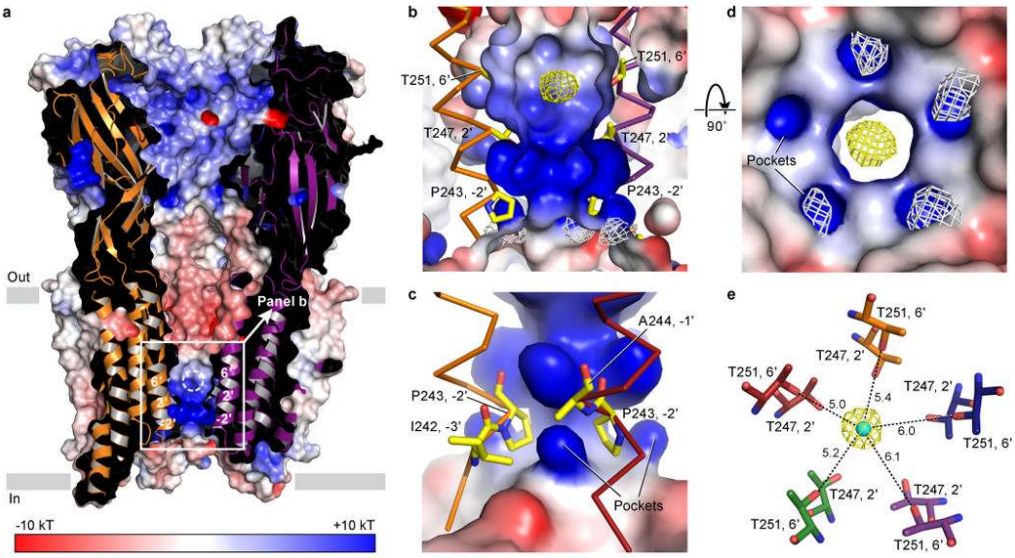

Figure 6. Ion selectivity

In **a**, front of receptor is cut away to reveal interior surface of pore, colored by electrostatic potential. Dashed circle in pore indicates putative chloride binding site. In **b**, expanded view from **a** showing selected M2 side chains from opposing subunits. Anomalous difference peaks at pore base are attributed to iodide binding sites (light grey mesh, contoured at 3.5 σ). F_{obs}-F_{calc} omit density for the putative chloride site is represented by yellow mesh contoured at 3 σ. The electropositive pockets where iodide ions bind are shown in **c**, viewed from inside the protein surface; four residues from adjacent M2 helices that coordinate the iodide sites are shown as sticks. In **d**, electropositive pockets viewed from the intracellular side. In **e**, putative chloride site viewed from extracellular side of pore with 6′Thr residues in foreground; F_{obs}-F_{calc} omit density (yellow) is contoured at 4 σ. Carbon atoms are colored by chain and chloride is represented by a 1 Å cyan sphere. Closest distances in Å from protein atoms to center of sphere are indicated by dashed lines from the 6′Thr side chain hydroxyl.